Research Article

Dalal A. Aloraini, Aljawhara H. Almuqrin, Kawa M. Kaky, M. I. Sayyed, and Mohamed Elsafi*

Radiation shielding capability and exposure buildup factor of cerium(IV) oxide-reinforced polyester resins

https://doi.org/10.1515/epoly-2023-0128
received August 20, 2023; accepted October 27, 2023

Abstract: The radiation shielding characteristics of the polyester resin composites reinforced with cerium(IV) oxide (CeO_2) have been studied. The prepared composites were pure polyester–resin (Poly/CeO_2-0), 90% per weight polyester resin and 10% CeO_2 (Poly/CeO_2-10), (Poly/CeO_2-30), (Poly/CeO_2-50), and (Poly/CeO_2-60). The linear attenuation coefficient (LAC) values for the free polyester and polyester samples with CeO_2 were experimentally measured compared with the XCOM data. The experimental LAC value was found to be 0.2377 cm^{-1} at 0.0595 MeV, which is in good agreement with the calculated value of 0.2454 cm^{-1}. Also, for the same sample, the experimental LAC was found to be 0.1034 cm^{-1} at 0.662 MeV, showing a good agreement with the calculated value of 0.1057 cm^{-1}. The LAC values for the free polyester, Pol/CeO_2-30, and Pol/CeO_2-60 are 1.43, 31.82, and 107.77 cm^{-1} at 0.015 MeV, respectively. The big difference in the LAC values between the composite with 0 and 60% CeO_2 is evident. The radiation shielding efficiency (RSE) of the polyester with different amounts of CeO_2 was experimentally measured at four energy values. Also, we extended the calculation of RSE at other energy values in the range of 0.015–15 MeV). The exposure buildup factor (EBF) values for the free CeO_2 sample and the samples with CeO_2 are calculated. The EBF is small at low energies, then increases, and attains a maximum value at moderate energy; the EBF shows a decreasing trend with an increase in the energy.

*** Corresponding author: Mohamed Elsafi,** Physics Department, Faculty of Science, Alexandria University, 21511 Alexandria, Egypt, e-mail: mohamedelsafi68@gmail.com
Dalal A. Aloraini, Aljawhara H. Almuqrin: Department of Physics, College of Science, Princess Nourah Bint Abdulrahman University, P.O.Box 84428, Riyadh 11671, Saudi Arabia
Kawa M. Kaky: Al-Nisour University College, Baghdad, Iraq
M. I. Sayyed: Department of Physics, Faculty of Science, Isra University, Amman, Jordan; Renewable Energy and Environmental Technology Center, University of Tabuk, Tabuk 47913, Saudi Arabia

Keywords: polyester, resin, cerium(IV) oxide, linear attenuation coefficient, radiation shielding efficiency, exposure buildup factor

1 Introduction

Gamma rays are a type of electromagnetic radiation characterized by high energy levels. In contemporary times, a potential hazard exists stemming from the exposure to unshielded ionizing radiation, which arises as a consequence of the widespread application of radiation in various domains of human activity, including industry, agriculture, research, medicine, and other domains renders it an indispensable component of our daily life. In order to fulfill the necessary criteria for mitigating the adverse effects of radiation, particularly for individuals operating inside radiation-prone areas, ongoing research endeavors are continuously progressing towards the development of appropriate materials for radiation shielding purposes (1,2).

This approach necessitates careful consideration of three key factors: the duration of exposure, the distance between the radiation source and the recipient, and the effectiveness of the shielding material utilized. The safeguarding of operators and equipment employed in environments with ionizing radiation has emerged as a significant area of study, aiming to mitigate the potential risks by developing improved shielding materials (3,4). The incidence of several diseases in human beings has been attributed to the long-term absorption of radioactive radiation. The increasing utilization of nuclear radiation in various technological applications has created a need for the development of engineered radiation shielding materials (5). Electromagnetic waves possess the distinct properties of being able to propagate across a vacuum without the need for a medium, maintaining a constant velocity equivalent to the speed of light. Photons, as elementary particles of electromagnetic radiation, possess both energy and momentum and are capable of exerting pressure (6).

In recent times, researchers have been actively engaged in exploring methods for the production of conditional absorbers as a means to address the limitations associated with conventional shielding absorbers. The utilization of polymer-based radiation defenses has garnered significant interest in various applications, mostly attributed to its advantageous characteristics of lightweight nature (7). The integration of polymer technology with lead shields has resulted in enhanced shielding capabilities compared to shields composed of alternative materials. Nevertheless, these shields are burdened by their substantial weight and the associated toxicity concerns (8).

Polyester exhibits a distinctive composition consisting of metallic and ceramic components, rendering it advantageous for many purposes. However, it is important to note that its shielding capability is significantly diminished in the absence of additions. Nevertheless, the use of additives, particularly heavy metals, significantly enhances the effectiveness of radiation shielding (9,10). Heavy metals such as tungsten trioxide (WO_3), lead oxide (PbO), molybdenum trioxide (MoO_3), bismuth trioxide (Bi_2O_3), and tellurium dioxide (TeO_2) exhibit a notable ability to provide shielding, enabling them to effectively reduce the effects of incoming radiation when compared to standard shielding materials (11). The macromolecular environment surrounding nanoparticles experiences modifications as a result of the notable surface-to-volume ratio that distinguishes nanoparticles from other materials (12,13).

Mechanical qualities, such as elastic stiffness, strength, and radiation shielding efficiency (RSE), are strengthened once nanoparticles are incorporated into the polymer matrix. Due to its exceptional capabilities and specific features, cerium oxide (CeO_2) is currently garnering substantial attention as a promising material for radiation shielding. The high atomic number of the CeO_2 combination gives it the capacity to effectively absorb gamma rays. CeO_2's dense arrangement is very good at both scattering and absorbing radiation, leading to a significant decrease in radiation transmission through the material (1,3,14). To top it off, CeO_2 is an ideal material for long-term protection due to its outstanding stability and resistance to radiation-induced damage. Furthermore, CeO_2 can be synthesized in various configurations, such as bulk and nanostructured materials, as well as thin films, hence providing versatility in the development and implementation of radiation shielding technologies. Additional study is needed to determine CeO_2's efficacy as a radiation shielding and nuclear safety material (15).

2 Materials and method

The prepared composites consist of two mean components, a matrix material called polyester resin with its hardener (where the hardener percentage represents 5% of the polyester resin quantity added; purchased from one of the paint stores in Egypt) and a CeO_2 as filler oxide with purity 98.9% (purchased from a chemical company in Egypt). The polyester resin properties were discussed in recent published papers (8–10). The CeO_2 had a density of 7.35 g·cm^{-3} and an average particle size of 20 ± 10 μm, and its characteristics were presented by Almutairi et al. (3). The preparation method was performed according to the percentages of polyester resin and CeO_2 in Table 1.

The two percentage components were mixed for 10 min to be a homogenous composite, and left in acceptable molds for 24 h for drying (16–19). Before attenuation measurements, the density of the CeO_2/Pol composites was determined using the mass-to-volume calculation (4), and the density values are given in Table 1. The density values were checked s by the Archimedes principle according to the following equation:

$$\rho(\text{g·cm}^{-3}) = \frac{W_C - W_L}{W_C}\rho_L \quad (1)$$

where W_C and W_L are the weights of the composite in dry air and immersing liquid, respectively, and $\rho_L = 1$ g·cm^{-3} is the density of the immersing liquid (water).

For attenuation measurements, the detector used was a high-purity germanium detector, the radioactive point sources were Am-241, Cs-137, and Co-60, and the characteristics of the detector and sources used are as presented in previous work (20–23). To get a narrow beam during the measurements, a lead collimator was used as shown in Figure 1. First, the detector was calibrated (energy calibration, efficiency calibration, and the sample position calibration between the detector and the point source) and then the point source was placed axially with the collimator and detector and click started within a certain time to form peaks related to the incoming energy photons emitted from the source (time makes the error percentage less than 1%). The area under these peaks can be calculated using Genie-2000 software, and the rate of this area (calculated area per measuring time) represents the intensity of

Table 1: Chemical composition of CeO_2/polyester composites

Composite code	Weight percentage, (wt%)		Density, (g·cm^{-3})
	Polyester resin	CeO_2	
Pol-CeO-0	100	0	1.310
Pol-CeO-10	90	10	1.427
Pol-CeO-30	70	30	1.738
Pol-CeO-50	50	50	2.221
Pol-CeO-60	40	60	2.580

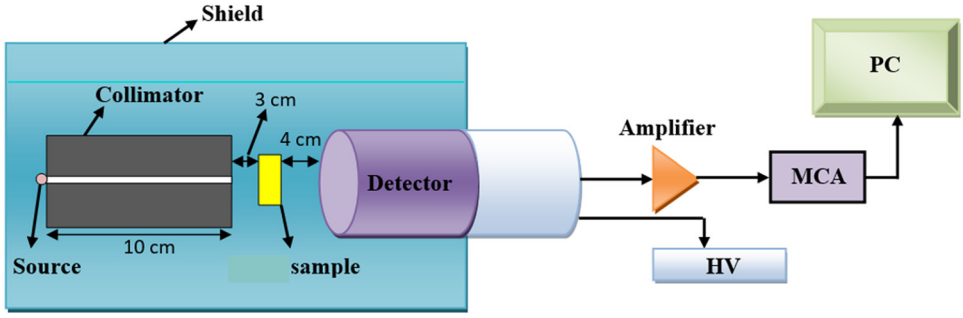

Figure 1: The geometry of the experimental work.

the incoming photon. We represent the intensity in the absence of the glass sample by the initial intensity (I_0), while by placing the glass sample between the detector and the point source, the calculated intensity is represented by the transmitted intensity (I_T). The variation of transmitted intensity depends on the incident energy photon, thickness, and density of the glass sample. From these intensities, the linear attenuation coefficient (LAC) of the glass sample of a thickness (t) can be evaluated by the formula (24–26),

$$\mathrm{LAC}(\mathrm{cm}^{-1}) = \frac{-1}{x} \ln \frac{I}{I_0} \tag{2}$$

The absorber parameters such as the half value layer (HVL), mean free path (MFP), and tenth value layer (TVL) are estimated as an inverse function of the LAC of the shield material as follows (27–33):

$$\mathrm{HVL, cm} = \frac{\ln(2)}{\mathrm{LAC}} \tag{3}$$

$$\mathrm{MFP, cm} = \frac{1}{\mathrm{LAC}} \tag{4}$$

$$\mathrm{TVL, cm} = \frac{\ln(10)}{\mathrm{LAC}} \tag{5}$$

The GP fitting parameters can be used to estimate the exposure buildup factor (EBF) values for any shielding microcomposite, where all equations used for the calculation of EBF are as in (34).

3 Results and discussion

The LAC values for the free polyester and for the polyester samples with CeO_2 were experimentally measured as we discussed in the previous section, and we compared the experimental values with the XCOM data (i.e. theoretical results). As shown in Figure 2(a–e), we presented this comparison for the free polyester and polyester with 10%, 30%, 50% and 60% CeO_2, respectively. Notable, we plotted the XCOM data at a wide energy of 0.015–15 MeV, while the experimental LAC values are determined only at four energies. The results shown in Figure 2 give the extent of the precision of the experimental setup used in this investigation since we can see good agreement between the experimental data (red circles) and the theoretical data of all composites. For example, as shown in Figure 2a, the experimental LAC value was found to be 0.2377 cm^{-1} at 0.0595 MeV, which is in good agreement with the calculated value of 0.2454 cm^{-1}. Also, for the same sample, the experimental LAC was found to be 0.1034 cm^{-1} at 0.662 MeV and shows good agreement with the calculated value of 0.1057 cm^{-1}. The deviation between both approaches is very small for all composites at any energy value, which confirms the accuracy of the experimental data. As shown in Figure 2b–e, the Kedge of CeO_2 (~40 keV) will appear and increase with increasing the CeO_2 concentration in the matrix, which causes higher absorption at this energy area. Also, the density increases with increasing the CeO_2 concentration in the matrix; then, the probability of gamma-ray interaction with the composite at a certain thickness increases.

As shown in Figure 2f, we plotted the LAC values for all composites to examine the role of changing the CeO_2 content on the LAC values. Apparently, the LAC values increase for the composites with the addition of CeO_2. The free CeO_2 polyester shows lower LAC values than the other composites, while the Pol/CeO_2-60 sample shows the highest LAC. We can correlate this outcome with the density of the composites. As the density increases with the addition of CeO_2, the increase in the LAC value results from the addition of CeO_2. Numerically, the LAC values for the free polyester, for Pol/CeO_2-30 and Pol/CeO_2-60 at 0.015 MeV are 1.43, 31.82, and 107.77 cm^{-1}, respectively. The high difference in the LAC values between the composites with 0 and 60% of CeO_2 is evident, At higher energy, we can observe that the LAC values decrease and attain the minimum values at 15 MeV.

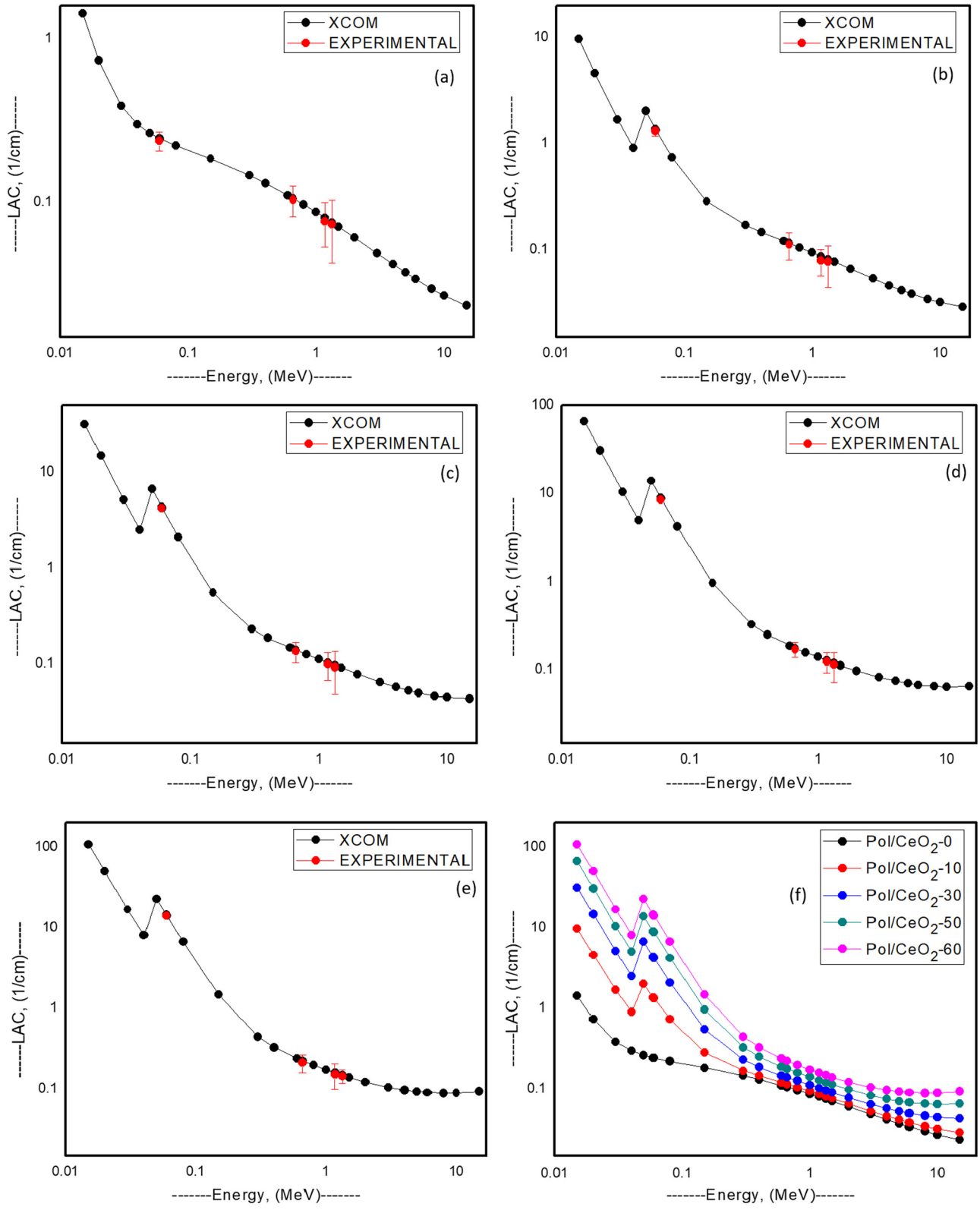

Figure 2: The LAC values of polyester–CeO_2 composites at different energies (MeV). (a) Pol/CeO2-0, (b) Pol/CeO2-10, (c) Pol/CeO2-30, (d) Pol/CeO2-50, (e) Pol/CeO2-60 and (f) All Pol/CeO2 composites.

For the previous three samples, the LAC values at 0.1 MeV are 0.208, 1.246, and 3.841 cm^{-1}. We can observe that the LAC is a function of energy and the difference in the LAC values due to the addition of CeO_2 decreases with increasing the energy. One important point to note from Figure 2f is that the peak is observed at 0.05 MeV for all composites, except for Pol/CeO_2-0, which is attributed to the K absorption edge of Ce. Since Pol/CeO_2-0 does not contain CeO_2, we did not observe the peak in LAC at 0.05 MeV. If we compared these results with the related work published in Ref. (30) where the iron filing was added as a filler with the resin, we observed an improvement in the present results; for example, at 0.662 MeV, the highest experimental LAC value for Pol-IF60 was 0.1948 cm^{-1} while the highest experimental value in this work was 0.2139 cm^{-1}.

In Figure 3(a) and 4(b), we plotted the theoretical HVL and MFP, respectively, while in Figures 3(b) and 4(b), we compared the theoretical and experimental HVL and MFP, respectively, and we showed the results at only four energy values (the energies emitted from the selected radioactive sources). Evidently, the experimental and calculated HVL for the prepared composites shows a close match, demonstrating a perfect agreement between the measured and theoretical data. The same holds for the MFP. From Figures 3 and 4(a), we can see that both HVL and MFP increase with increasing energy (35,36). The measured HVL for the prepared composites at 0.059 MeV are 2.74, 0.49, 0.16, 0.073, and 0.046 cm for the free polyester and polyester with 10%, 30%, 50%, and 60% CeO_2 respectively. The effect of CeO_2 on the HVL for these composites is at 0.059 MeV, where the HVL greatly reduced from 2.74 to 0.046 cm due to the addition of 60% CeO_2. At the same energy, we found that CeO_2 also greatly affects the MFP, where the MFP reduces from 3.94 to 0.067 cm due to the addition of 60% CeO_2 to the polyester. At higher energy (0.662 MeV), we found that the HVL decreases from 6.41 cm (for Pol/CeO_2-0) to 2.92 cm (for Pol/CeO_2-60). Similar studies reported a decrease in the HVL due to the addition of heavy metal elements (37,38). From these results, we can conclude that the HVL at 0.662 MeV is reduced by a factor of approximately 2.19 when we added 60% CeO_2 to the polyester. Also, we can conclude that the thickness of the polyester must be higher than 2.92 cm to attenuate 50% of the intensity of the photons emitted from ^{137}Cs. From the MFP data at 0.662 MeV, we found that the free polyester sample has an MFP of 12.41 cm, decreasing to 11.52 cm due to the addition of 10% CeO_2 and decreasing to 6.23 cm when 60% CeO_2 is added to the polyester, which indicates that the MFP is also decreased by a factor of about 2 due to the addition of 60% CeO_2. At higher energy, for example, 1 MeV, we found that the HVL for the prepared samples is of the order of 7.95–3.94 cm, while the MFP is of the order of 11.47–5.69 cm.

The RSE of the polyester with different amounts of CeO_2 was experimentally measured at four energy values. Also, we extended the calculation of RSE at other energy values (in the range of 0.015–15 MeV). In Figure 5a, we plotted the RSE in a wide energy range, while in Figure 5b we plotted the measured RSE at four energy values and compared the experimental values with the theoretical ones. Apparently, a good agreement is reported between the experimental and theoretical RSE at the selected

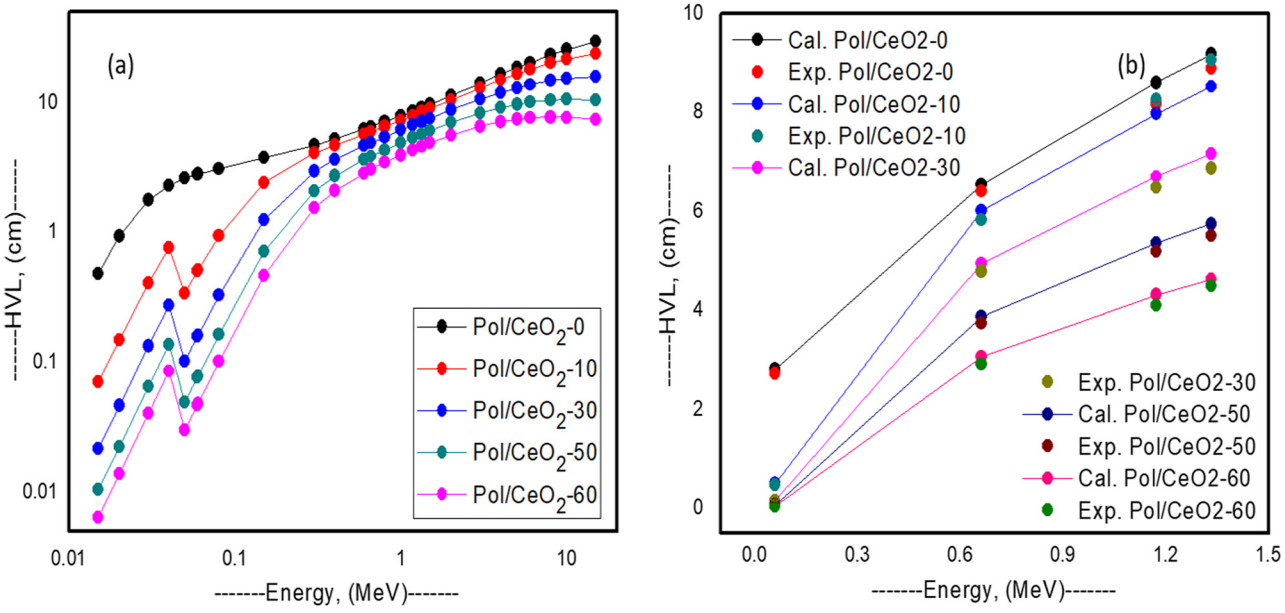

Figure 3: The experimental and theoretical HVL of the polyester–CeO_2 composites at different energies, (a) Theoretical values and (b) Comparison between the experimental and theoretical values.

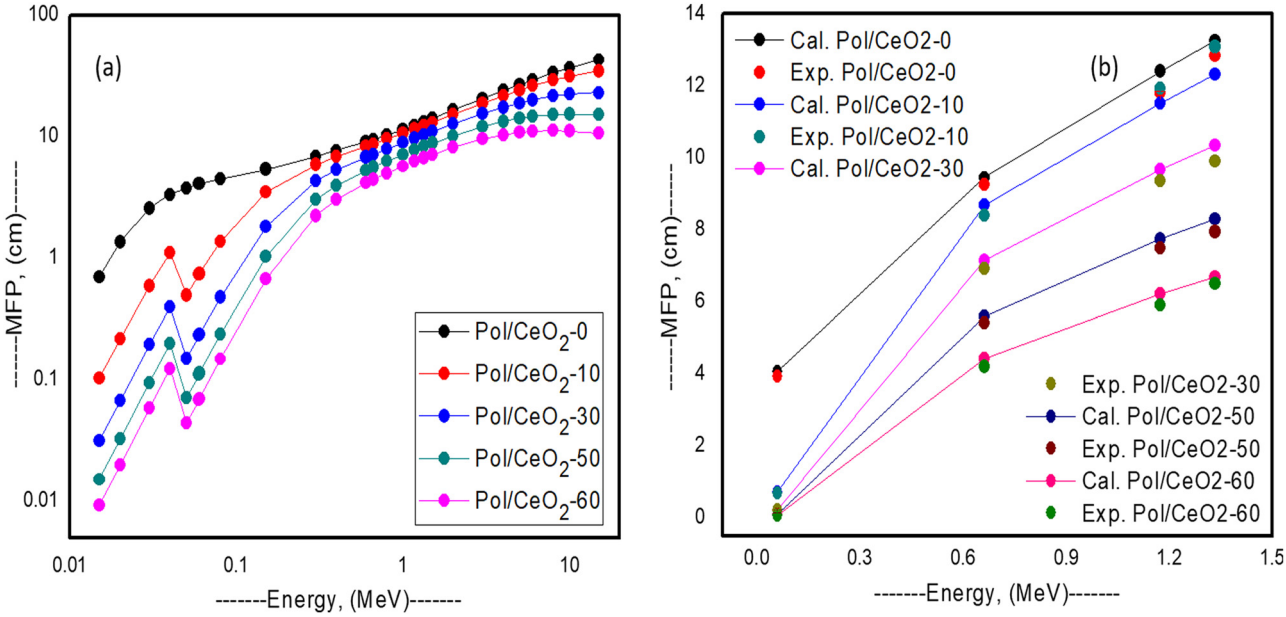

Figure 4: The experimental and theoretical MFP of the polyester–CeO_2 composites at different energies, (a) Theoretical values and (b) Comparison between the experimental and theoretical values.

energies (Figure 5b). At 0.015 MeV, the RSE for all composites is 100%, which means that all composites can block all the photons with an energy of 0.015 MeV. The remarkable 100% RSE reported at 0.015 MeV underscores the exceptional low-energy photon-shielding abilities of the prepared composites, likely ascribed to the presence of high-*Z* elements (such as Ce) within its composition. At 0.02 and 0.03 MeV, the polyester composites with CeO_2 also have a perfect shielding efficiency, where the RSE is also 100%. At higher energies, the RSE decreases, which indicates that the ability of these composites to attenuate the radiation is decreased. The reduction in RSE with increasing energy can be attributed to the decreased interaction and hence increased penetration of photons via the composites. The CeO_2 also affected the RSE and thus it is important to consider high amounts of CeO_2 during the preparation process in order to obtain suitable radiation shielding materials. Clearly, a higher RSE corresponds to the maximum amount

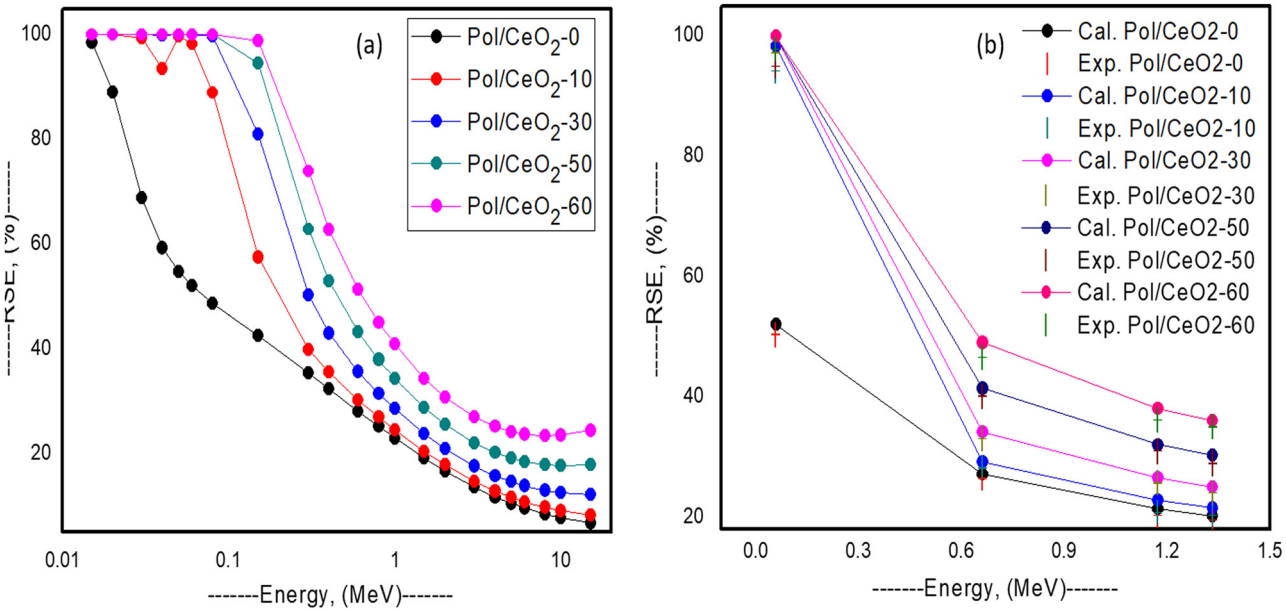

Figure 5: The experimental and theoretical RSE of the polyester–CeO_2 composites at different energies, (a) Theoretical values and (b) Comparison between the experimental and theoretical values.

of CeO_2. Also, the free CeO_2 composite has a lower RSE than the other composites, which indicates that the RSE is directly proportional to the CeO_2 amount. Numerically, the RSE at 0.662 MeV for the free CeO_2 composite is 27.18%, which increases to 29.19% for Pol/CeO_2-10, and to 34.28% for Pol/CeO_2-30, while the maximum RSE at this energy is found for Pol/CeO_2-60 (49.12%). The incorporation of CeO_2 increases the RSE since cerium (Ce) has a high atomic number (Z = 58), which results in stronger interactions with the incoming photons and enhanced attenuation abilities within the composites.

The effective atomic number (Z_{eff}) is a useful parameter in radiation shielding. As radiation shielding materials are composed of different elements, we can examine the impact of the weight fraction of the different elements on the radiation attenuation performance using this parameter. In Figure 6, we plotted Z_{eff} for the prepared composites as a function of energy. For Pol/CeO_2-0, Z_{eff} is almost constant and varied between about 4 and 6. This is because the polyester is composed of elements with low atomic numbers, and this sample does not contain CeO_2. However, the addition of CeO_2 causes a significant improvement in the Z_{eff}. Z_{eff} for the polyester with 10%, 30%, 50%, and 60% CeO_2 is higher than the Z_{eff} for free CeO_2. The composite with a high amount of CeO_2 has an elevated Z_{eff} due to the significant contribution of Ce owing to its high atomic number, which causes an enhanced overall atomic number for the prepared samples, improving their radiation shielding features (39,40). Moreover, at a low energy range, a big difference in the Z_{eff} between the different composites is observed. The high differences in Z_{eff} among the glasses in the low-energy region can be ascribed to variations in their elemental compositions, with composites containing high amounts of

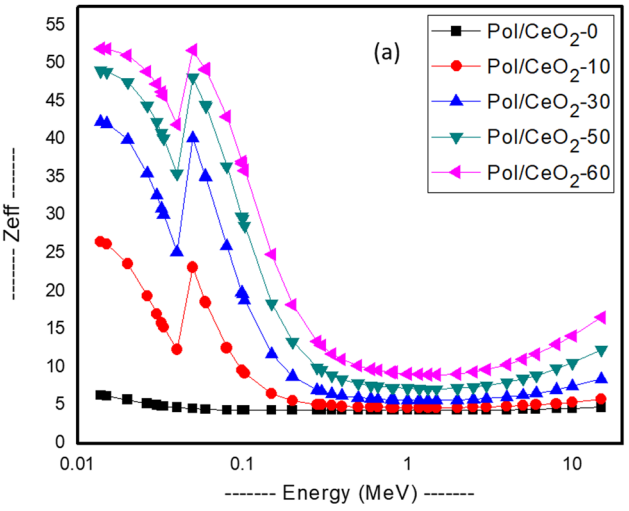

Figure 6: (a) The Z_{eff} of the polyester–CeO_2 composites at different energies.

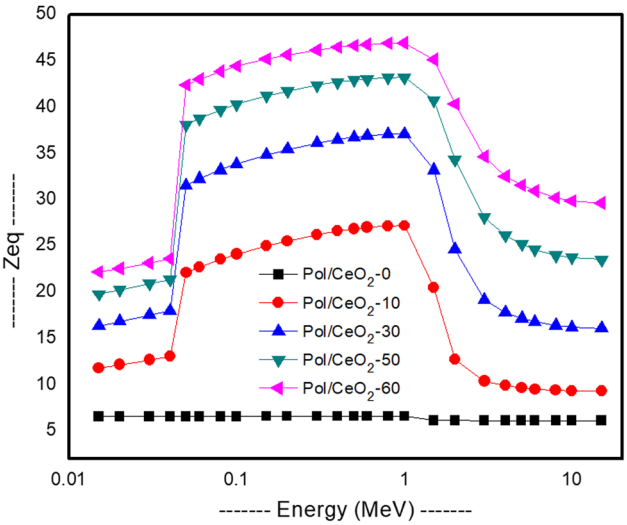

Figure 7: The Z_{eq} of the polyester–CeO_2 composites at different energies.

CeO_2 contributing highly to Z_{eff} due to their improved interaction with low-energy photons. For example, the Z_{eff} values for polyester with 0 and 60% CeO_2 at 0.015 MeV are 6.39 and 51.94, while at 0.03 MeV, the Z_{eff} values for the same two composites are 5.06 and 47.32. Therefore, significant enhancement in the Z_{eff} is observed at a low energy owing to the dominant photoelectric effect at this energy range. At higher energies, the difference in the Z_{eff} between the different composites becomes small owing to the dominant Compton scattering and pair production.

The equivalent atomic number (Z_{eq}) values were determined to calculate the buildup factor (EBF). The Z_{eq} data is plotted in Figure 7. We found the addition of CeO_2 causes an increase in the Z_{eq}. Z_{eq} is a useful parameter to calculate the EBF, and the results of EBF for the free CeO_2 sample and the samples with CeO_2 are shown in Figure 8. The EBF is small at low energies, then increases and attains a maximum value at moderate energy; EBF shows a decreasing trend with increasing energy. Apparently, a peak is formed in the EBF for the samples with CeO_2 around 0.05 MeV, which is attributed to the K absorption edge of CeO_2. Moreover, the EBF shows an increasing trend with an increase in the MFP, where the maximum EBF is found at 40 mfp.

4 Conclusion

In this study, radiation attenuation as well as buildup factor of different composites consisting of polyester resin materials and curium oxide have been investigated. The experimental LAC value is in good agreement with the calculated value, which indicates that the deviation

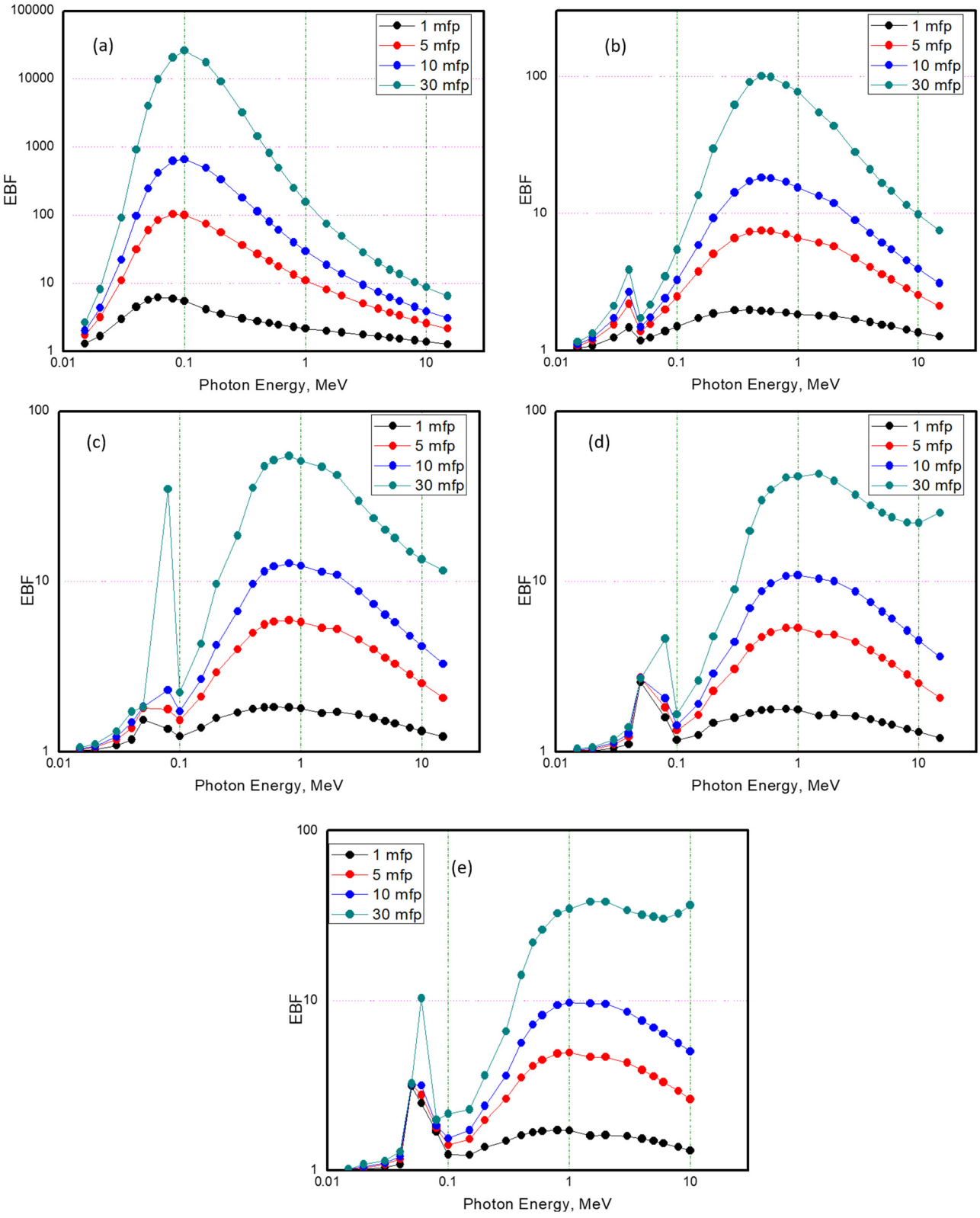

Figure 8: The EBF of the polyester–CeO_2 composites at different MFP values, (a) Pol/CeO_2-0, (b) Pol/CeO_2-10, (c) Pol/CeO_2-30, (d) Pol/CeO_2-50, and (e) Pol/CeO_2-60.

between both approaches is very small for all composites at any energy and confirms the accuracy of the experimental data. The effect of CeO_2 on the HVL for these composites is at 0.059 MeV, where the HVL greatly reduced from 2.74 to 0.046 cm due to the addition of 60% CeO_2. At the same energy, we found that CeO_2 also highly affects the MFP, where the MFP reduces from 3.94 to 0.067 cm due to the addition of 60% CeO_2 to the polyester. The RSE enhances significantly when transitioning from Pol/CeO_2-0 to Pol/CeO_2-60, or when 60% CeO2 is added. At higher energies, the difference in the Z_{eff} between the different composites become small owing to the dominant Compton scattering and pair production. The EBF is small at low energies, then increases and attains a maximum value at moderate energy; the EBF then shows a decreasing trend with increasing energy. Apparently, a peak appears in the EBF for the samples with CeO_2 at around 0.05 MeV.

Funding information: Authors state no funding involved.

Conflict of interest: Authors state no conflict of interest.

References

(1) Rahman MM, Suleiman R, Zahir MH, Helal A, Kumar AM, Haq MB. Multi Self-healable UV shielding polyurethane/CeO2 protective coating: the effect of low-molecular-weight polyols. Polymers. 2020;12(9):1947.

(2) Eyssa HM, Sadek RF, Mohamed WS, Ramadan W. Structure property behavior of polyethylene nanocomposites containing Bi_2O_3 and WO_3 as an eco-friendly additive for radiation shielding. Ceram Int; 2023;49:18442–54.

(3) Almutairi HM, Al-Saleh WM, Abualsayed MI, Elsafi M. Effect of cerium(IV) oxide particle size on polydimethylsiloxane polymer to form flexible materials against ionizing radiation. Polymers. 2023;15(13):2883.

(4) Sayyed MI, Yasmin S, Almousa N, Elsafi M. The radiation shielding performance of polyester with TeO2 and B2O3. Processes. 2022;10(9):1725.

(5) Sallam FH, Tharwat M, Almuqrin AH, Sayyed MI, Mahmoud KA. Ni0.5Zn0.5Fe2O4 nanoparticles reinforced polyester composite for advanced radiation shielding applications: A detailed discussion for synthesis, characterization, and gamma-ray attenuation properties. Radiat Phys Chem. 2023;208:110907.

(6) Kassem SM, Maksoud MA, Ghobashy MM, El Sayed AM, Ebraheem S, Helal AI, et al. Novel flexible and lead-free gamma radiation shielding nanocomposites based on LDPE/SBR blend and BaWO4/B2O3 heterostructures. Radiat Phys Chem. 2023;209:110953.

(7) Alresheedi MT, Elsafi M, Aladadi YT, Abas AF, Ganam AB, Sayyed MI, et al. Assessment of silicone rubber/lead oxide composites enriched with Bi [sub. 2] O [sub. 3], WO [sub. 3], BaO, and SnO [sub. 2] nanoparticles for radiation shielding applications. Polymers. 2023;15(9):2160.

(8) Sayyed MI, Almurayshid M, Almasoud FI, Alyahyawi AR, Yasmin S, Elsafi M. Developed a new radiation shielding absorber composed of waste marble, polyester, PbCO3, and CdO to reduce waste marble considering environmental safety. Materials. 2022;15(23):8371.

(9) Almuqrin AH, Yasmin S, Abualsayed MI, Elsafi M. An experimental investigation into the radiation-shielding performance of newly developed polyester containing recycled waste marble and bismuth oxide. Appl Rheol. 2023;33(1):20220153.

(10) Almuqrin AH, Yasmin S, Abualsayed MI, Elsafi M. Grafting of heavy metal oxides onto pure polyester for the interest of enhancing radiation shielding performance. Radiochim Acta. 2023;111(6):495–502.

(11) Liman ML, Islam MT, Hossain MM. Mapping the progress in flexible electrodes for wearable electronic textiles: materials, durability, and applications. Adv Electron Mater. 2022;8(1):2100578.

(12) Dong M, Zhou S, Xue X, Feng X, Yang H, Sayyed MI, et al. Upcycling of boron bearing blast furnace slag as highly cost-effective shield for protection of neutron radiation hazard: An innovative way and proposal of shielding mechanism. J Clean Prod. 2022;355:959–6526.

(13) Haji A, Rahbar RS, Shoushtari AM. Improved microwave shielding behavior of carbon nanotube-coated PET fabric using plasma technology. Appl Surf Sci. 2014;311:593–601.

(14) Tishkevich DI, Rotkovich AA, German SA, Zhaludkevich AL, Vershinina TN, Bondaruk AA, et al. Heavy alloy based on tungsten and bismuth: fabrication, crystal structure, morphology, and shielding efficiency against gamma-radiation. RSC Adv. 2023;13:24491. doi: 10.1039/D3RA04509A.

(15) Aloraini DA, Almuqrin AH, Sayyed MI, Kumar A, Gaikwad DK, Tishkevich DI, et al. Experimental and theoretical analysis of radiation shielding properties of strontium-borate-tellurite glasses. Opt Mater. 2021;121:925–3467.

(16) Sayyed MI, Al-Ghamdi H, Almuqrin AH, Yasmin S, Elsafi M. A study on the gamma radiation protection effectiveness of nano/micro-mgo-reinforced novel silicon rubber for medical applications. Polymers. 2022;14(14):2867. doi: 10.3390/polym14142867.

(17) Hannachi E, Sayyed MI, Yassine S, Elsafi M. Experimental investigation on the physical properties and radiation shielding efficiency of YBa2Cu3Oy/M@M3O4 (M = Co, Mn) ceramic composites. J Alloy Compd. 2022;904:164056.

(18) Al-Ghamdi H, Elsafi M, Almuqrin AH, Yasmin S, Sayyed MI. Investigation of the gamma-ray shielding performance of CuO-CdO-Bi_2O_3 bentonite ceramics. Materials. 2022;15(15):5310.

(19) Al-Ghamdi H, El-Nahal MA, Saleh IH, Sayyed MI, Almuqrin AH. Determination of ^{238}U and ^{40}K radionuclide concentrations in some granite rocks by gamma spectroscopy and energy dispersive X-ray analysis. Materials. 2022;15(15):5130.

(20) Sayyed MI, Hashim S, Hannachi E, Slimani Y, Elsafi M. Effect of WO_3 nanoparticles on the radiative attenuation properties of $SrTiO_3$ perovskite ceramic. Crystals. 2022;12(11):1602.

(21) Sayyed MI, Almurayshid M, Almasoud FI, Yasmin S, Elsafi M. Developed a new radiation shielding absorber composed of waste marble, polyester, $PbCO_3$, and CdO to reduce waste marble considering environmental safety. Materials. 2022;15(23):8371.

(22) Aloraini DA, Elsafi M, Almuqrin AH, Sayyed MI. Coincidence summing factor calculation for volumetric γ -ray sources using geant4 simulation. Sci Technol Nucl Install. 2022;2022:5718920.

(23) D'Souza AN, Padasale B, Murari MS, Almuqrin AH, Kamath SD. TeO_2 for enhancing structural, mechanical, optical, gamma and neutron radiation shielding performance of bismuth borosilicate glasses. Mater Chem Phys. 2023;293:126657.

(24) Hannachi E, Sayyed MI, Slimani Y, Elsafi M. Structural, optical and radiation shielding peculiarities of strontium titanate ceramics mixed with tungsten nanowires: An experimental study. Opt Mater. 2023;135:113317.
(25) Elsafi M, Almousa N, Al-Harbi N, Yasmin S, Sayyed MI. Ecofriendly and radiation shielding properties of newly developed epoxy with waste marble and WO_3nanoparticles. J Mater Res Technol. 2023;22:269–77.
(26) Hannachi E, Sayyed MI, Slimani Y, Baykal A, Elsafi M. Structure and radiation-shielding characteristics of BTO/MnZnFeO ceramic composites. J Phys Chem Solids. 2023;174:111132.
(27) Elsafi M, Al-Ghamdi H, Sayyed MI, Shalaby TI, El-Khatib AM. Optimizing the gamma-ray shielding behaviors for polypropylene using lead oxide: A detailed examination. J Mater Res Technol. 2022;19:1862–72.
(28) Sayyed MI, Almousa N, Elsafi M. Green conversion of the hazardous cathode ray tube and red mud into radiation shielding concrete. Materials. 2022;15(15):5316.
(29) Almuqrin AH, Elsafi M, Yasmin S, Sayyed MI. Morphological and gamma-ray attenuation properties of high-density polyethylene containing bismuth oxide. Materials. 2022;15(18):6410.
(30) Al-Saleh WM, Dahi MR, Sayyed MI, Almutairi HM, Saleh IH, Elsafi M. Comprehensive study of the radiation shielding feature of polyester polymers impregnated with iron filings. e-Polymers. 2023;23(1):20230096. doi: 10.1515/epoly-2023-0096.
(31) Alorain DA, Almuqrin AH, Sayyed MI, Elsafi M. Impact of WO_3 and BaO nanoparticles on the radiation shielding characteristics of polydimethylsiloxane composites. e-Polymers. 2023;23(1):20230037. doi: 10.1515/epoly-2023-0037.
(32) Elsafi M, Almuqrin AH, Yasmin S, Sayyed MI. The affinity of bentonite and WO_3 nanoparticles toward epoxy resin polymer for radiation shielding. e-Polymers. 2023;23(1):20230011. doi: 10.1515/epoly-2023-0011.
(33) Wu B, Zhu H, Yang Y, Huang J, Liu T, Kuang T, et al. Effect of different proportions of CNTs/Fe_3O_4 hybrid filler on the morphological, electrical and electromagnetic interference shielding properties of poly(lactic acid) nanocomposites. e-Polymers. 2023;23(1):20230006. doi: 10.1515/epoly-2023-0006.
(34) Alresheedi MT, Elsafi M. Effect of waste Iron Filings (IF) on radiation shielding feature of polyepoxide composites. Crystals. 2023;13:1168. doi: 10.3390/cryst13081168.
(35) Saleh A. Comparative shielding features for X/Gamma-rays, fast and thermal neutrons of some gadolinium silicoborate glasses. Prog Nucl Energy. 2022;154:104482.
(36) Saleh A, Shalaby RM, Abdelhakim NA. Comprehensive study on structure, mechanical and nuclear shielding properties of lead free Sn–Zn–Bi alloys as a powerful radiation and neutron shielding material. Radiat Phys Chem. 2022;195:110065.
(37) Sayyed MI. The role of Bi2O3 on radiation shielding characteristics of ternary bismuth tellurite glasses. Optik. 2022;270:169973.
(38) Saleh A, El-Feky MG, Hafiz MS, Kawady NA. Experimental and theoretical investigation on physical, structure and protection features of TeO2-B2O3 glass doped with PbO in terms of gamma, neutron, proton and alpha particles. Radiat Phys Chem. 2022;202:110586.
(39) Bilici S, Kamislioglu M, Guclu EEA. A Monte Carlo simulation study on the evaluation of radiation protection properties of spectacle lens materials. Eur Phys J Plus. 2023;138(1):80.
(40) Kamislioglu M. An investigation into gamma radiation shielding parameters of the (Al:Si) and (Al + Na):Si-doped international simple glasses (ISG) used in nuclear waste management, deploying Phy-X/PSD and SRIM software. J Mater Sci Mater Electron. 2021;32:12690–704.